

Transient Electric Birefringence Study of Intermediate Filament Formation from Vimentin and Glial Fibrillary Acidic Protein*

(Received for publication, April 17, 1997, and in revised form, June 27, 1997)

Martin Kooijman‡, Michael Bloemendal‡, Peter Traub§, Rienk van Grondelle‡, and Herbert van Amerongen‡¶

From the ‡Department of Physics and Astronomy and Institute for Molecular Biological Sciences, Vrije Universiteit, De Boelelaan 1081, 1081 HV Amsterdam, The Netherlands and the §Max Planck Institute for Cell Biology, D68526 Ladenburg/Heidelberg, Germany

Mg²⁺-induced polymerization of type III intermediate filament proteins vimentin and glial fibrillary acidic protein was studied by transient electric birefringence. In the absence of MgCl₂ we found a net permanent dipole moment, ~45-nm-long dimers for vimentin, ~65-nm-long tetramers, hexamers, and possibly octamers for both proteins, and 100-nm aggregates for glial fibrillary acidic protein. Controlled oligomerization occurred after the addition of MgCl₂. Although the solutions contained (small) aggregates of different sizes, more or less discrete steps in polymer formation were observed, and it was possible to discriminate between an increase in width and length. At the first stage of polymerization (in 0.3 mM MgCl₂ for vimentin and 0.2 mM MgCl₂ for glial fibrillary acidic protein), the permanent dipole moment disappeared without a change in length of the particles. At higher MgCl₂ concentrations, structures of approximately 100 nm were formed, which strongly tended to laterally assemble into full-width intermediate filament structures consisting of about 32 monomers. This contrasts with previous models where first full-width (~10-nm) aggregates are formed, which then increase in length. Subsequently, two discrete elongation steps of 35 nm are observed that increase the length to 135 and 170 nm, respectively. Possible structural models are suggested for the polymerization.

Many eukaryotic cells contain cytoplasmic intermediate filaments (IFs),¹ which are composed of proteins with a molecular mass of 40–210 kDa (1, 2). All IF proteins contain a central α -helix-rich region, consisting of approximately 310 amino acids, flanked by nonhelical amino- and carboxy-end domains, which are extremely diverse in size, composition, and charge characteristics.

The α -helical regions of two IF protein chains assemble parallel and exactly in register to form a 45-nm coiled-coil rod with end domains of uncertain length (2–4). In a recent publication on vimentin IF structures, we have proven the occurrence of such dimers in low ionic strength solution (5). We have also shown that these rods are bent and/or flexible structures (7).

In the late eighties and early nineties, much work was done to elucidate the next level of IF organization (5, 8–23). Most of these studies have been reviewed by Heins and Aebi (2). At the level of tetramers, essentially four alignments of the constituting dimers have been suggested: antiparallel in register forming a rod approximately 45 nm long, head-to-tail with slight overlap and antiparallel staggered in two different ways, yielding a rod length of approximately 65 nm. Together with other data (9–11), our transient electric birefringence (TEB) data on vimentin missing the first 70 amino acids (T-vimentin) (24), intact vimentin (6), desmin, and glial fibrillary acidic protein (GFAP) (7) provided evidence for the predominant occurrence of the latter. Moreover, we detected particles with a length very similar to that of staggered tetramers but with a much larger permanent dipole moment (6, 7). Most likely, these represent hexamers as suggested by Steinert (10, 11) and Herrmann *et al.* (15).

Conflicting models for the molecular architecture of higher oligomers have been suggested (2, 12, 19, 21), and intermediate steps in filament formation are not well understood (17, 21). As mentioned by Heins and Aebi (2) “the hierarchy of the three types of lateral dimer-dimer interaction is ambiguous in these models.” Furthermore, it is not clear what the exact number of IF monomers in filament cross-section is, this may be varying in different filaments and even within the same filament (2, 22, 25).

Most evidence for current ideas on IF assembly is based on EM results and cross-linking studies. The latter give very detailed information on the connections between amino acids of different protein subunits, but the hierarchy of dimer-dimer interactions in IFs cannot be deduced from them, the size distribution of the oligomers is unknown, and direct evidence for higher structures is not obtained. To verify postulated models in solution and to obtain more information on three-dimensional growth and organization of IFs, we have performed a TEB study on MgCl₂-induced filament formation of the type III IF proteins vimentin and GFAP. To our knowledge, this is the first detailed study on the architecture of complete glial filaments, the paper by Stewart *et al.* (26) on the rod portion of GFAP being the only other detailed structural study on this protein.

EXPERIMENTAL PROCEDURES

Sample Preparation

Vimentin from Ehrlich ascites tumor cells and GFAP from bovine brain white matter, purified as described (27), lyophilized, and stored at –20 °C, was dissolved in 2 mM phosphate, pH 7.5, 6 mM 2-mercaptoethanol, 6 M urea. From this buffer, the proteins were dialyzed at 4 °C for at least 16 h against 0.7 mM sodium phosphate, pH 7.5, 6 mM 2-mercaptoethanol (vimentin), and 2 mM BisTris-HCl, pH 6.8, 6 mM 2-mercaptoethanol (GFAP). The vimentin and GFAP concentrations in the absence of MgCl₂ were determined from the absorption using a

* This work was supported by the Netherlands Organization of Scientific Research, in part via the Foundation of Life Sciences. The costs of publication of this article were defrayed in part by the payment of page charges. This article must therefore be hereby marked “advertisement” in accordance with 18 U.S.C. Section 1734 solely to indicate this fact.

¶ To whom correspondence should be addressed. Tel.: 31 204447932; Fax: 31 204447899; E-mail: herbert@nat.vu.nl.

¹ The abbreviations used are: IF, intermediate filaments; TEB, transient electric birefringence; GFAP, glial fibrillary acidic protein; Ω , ohm; SI, sample interval.

molar extinction coefficient (ϵ) (per polypeptide chain) at 280 nm of 24,240 $\text{M}^{-1} \text{cm}^{-1}$ for vimentin and 20,100 $\text{M}^{-1} \text{cm}^{-1}$ for GFAP, calculated from the extinction coefficients of the individual tryptophan ($\epsilon = 6300 \text{M}^{-1} \text{cm}^{-1}$) and tyrosine ($\epsilon = 1380 \text{M}^{-1} \text{cm}^{-1}$) residues (28). Protein concentrations were adjusted to 0.08–0.14 mg/ml.

Transient Electric Birefringence

Theoretical Background—When dissolved optically anisotropic molecules are oriented by a square electric-field pulse, the solution becomes birefringent. When the field is switched off, the order and hence the birefringence decays by rotational diffusion with a rate that depends on the size and the shape of the molecules. From the accurately measurable time-resolved birefringence, the following parameters can be determined.

1) The ratio of the areas enclosed by the rise and decay curve of the birefringence, S_1/S_2 (see Fig. 1), which is related to the relative magnitudes of the permanent (P) and induced (Q) dipole moments of the particles according to Ref. 29.

$$\frac{S_1}{S_2} = \left(\frac{P}{4Q} + 1 \right) / \left(\frac{P}{Q} + 1 \right) \quad (\text{Eq. 1})$$

2) The Kerr constant (K), which is defined as the proportionality constant between the magnitude of the steady-state birefringence, Δn_0 , and the square of the electric field E ($K = \Delta n_0/E^2$) at low fields; K is proportional to the product of $P + Q$ and the optical anisotropy factor of the molecule.

3) The field-free decay time τ of the birefringence signal, yielding information on size and flexibility of the molecules (29). In a multispecies system, the average decay time τ_{av} is given by the equation,

$$\tau_{av} = \frac{\sum_i c_i K_i \tau_i}{\sum_i c_i K_i} \quad (\text{Eq. 2})$$

where c_i and K_i are the concentration and Kerr constant of species i with decay time τ_i .

Here we treat the filament aggregates as rigid cylindrical rods. For such particles, τ equals $1/(6D_r)$, where D_r is the end-over-end rotational diffusion coefficient (s^{-1}). Several expressions for D_r have been developed (30–32). D_r is strongly dependent on the length and rather insensitive to changes in the diameter.

Measurements—The electric birefringence setup has been described in detail (33). The field strength was varied between 0.3 and 4.0 kV/cm, the pulse width between 70 and 500 μs , and the sample interval between 0.1 and 1.0 μs . At least one early experiment was repeated at the end of a series to ensure that the samples remained intact. For each birefringence curve, at least 100 transients were averaged. Field strengths were determined by averaging five electric field pulses. Measurements were performed at 20 $^\circ\text{C}$.

To study the assembly of GFAP and vimentin IF under the influence of MgCl_2 (or NaCl), small aliquots of a 20 mM stock solution were added to the protein solution (volume 0.8 ml) and mixed using a Pasteur pipette. Transients were measured after 10 min and repeated until the TEB signal was constant. Conductivity of the samples was determined by measuring the impedance of the solution in the Kerr cell at 1 kHz (Fluke Impedance Bridge model 710B). The resistance of the solution ranged from $400 \pm 100 \Omega$ in the absence of MgCl_2 to approximately 80 Ω at 2.5 mM MgCl_2 .

The Kerr constants were determined in solutions with a resistance of 200 Ω by dialysis of the proteins from the aqueous low salt buffers (0.7 mM sodium phosphate, pH 7.5, and 2 mM BisTris-HCl, pH 6.8) to buffers with different concentrations of MgCl_2 (see Table I). The resistance was then adjusted to 200 Ω with NaCl , which did not change the birefringence decay signals. For vimentin at 1 mM MgCl_2 , where the resistance of the solution was 140 Ω only, a correction of the Kerr constant to 200- Ω solutions was made. Since the Kerr constants of vimentin at pH 8.5 and T-vimentin at pH 7.5 (in the presence and absence of MgCl_2) were approximately 30% smaller at 140 than at 200 Ω , the corrected K value for vimentin at 1 mM MgCl_2 as presented in Table I is 50% larger than the measured one.

Data Analysis—Steady-state birefringence was determined by averaging the plateau of the rise curve. The field-free decay of the birefringence was analyzed on a SUN4 workstation using the computer programs DISCRETE (34, 35) and CONTIN (36, 37). The former fits data with discrete exponential decays, while the latter uses a continuous

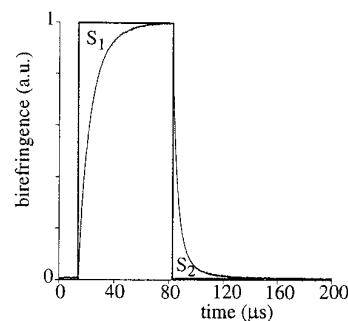


FIG. 1. Birefringence signal for vimentin in 0.7 mM sodium phosphate buffer, pH 7.5; $E = 1.2 \text{ kV/cm}$; pulse length, 70 μs . S_1 and S_2 are the areas enclosed by the rise and decay curves, respectively (see “Experimental Procedures”).

distribution of exponential decay times. In this paper we predominantly present results obtained from the analysis with DISCRETE, but in all cases the data were also analyzed with CONTIN to ensure that consistent results were obtained. Analyses were started 0.20 μs (when the sample interval (SI) = 0.1 or 0.2 μs), 0.50 μs (SI = 0.5 μs), or 1.0 μs (SI = 1.0 μs) after the orienting field was turned off.

RESULTS

The TEB signal of vimentin at pH 7.5 in the absence of MgCl_2 is shown in Fig. 1. The S_1/S_2 value (2.1 ± 0.1) is somewhat lower than that reported previously for vimentin at pH 6.8 and 8.5 (6), presumably due to the use of a slightly different buffer. When 0.3 mM MgCl_2 is added, S_1/S_2 decreases from 2.1 ± 0.1 to 1.1 ± 0.1 (Table I), showing that the permanent dipole moment has almost disappeared. Such a decrease is not observed when MgCl_2 is replaced by NaCl under conditions of equal sample resistance, reflecting a specific role of Mg^{2+} . The Kerr constant of vimentin in the absence of MgCl_2 is $1.2 \pm 0.2 \times 10^{-13} \text{ m}^2 \text{V}^{-2}$ for 1 M protein chain, a value comparable with that at pH 6.8 and 8.5 (6). The addition of 0.3 mM MgCl_2 does not change the Kerr constant to a large extent (Table I). For GFAP at pH 6.8, the effect of small amounts of MgCl_2 (0.2 mM) on S_1/S_2 is comparable with that for vimentin (a decrease from 1.5 ± 0.2 to 1.2 ± 0.1 ; see Table I), while NaCl did not result in such a decrease. The Kerr constant of GFAP is not affected between 0 and 0.2 mM MgCl_2 (Table I).

Raising the MgCl_2 concentration from 0.3 to 1.0 mM for vimentin and from 0.2 to 0.5 mM for GFAP leads to an increase of K by a factor of 15 and 12, respectively (Table I). On the other hand, the S_1/S_2 values of both proteins are not affected. At higher MgCl_2 concentrations, no steady-state birefringence could be reached; thus, no Kerr constants and S_1/S_2 values could be estimated.

CONTIN and DISCRETE analyses of the birefringence decay signals of vimentin (after 70- μs pulses) and GFAP (after 140- μs pulses) are presented in Tables II and III. For clarity, the decay processes in the tables have been denoted $\tau_1 \dots \tau_6$ (Table II) or $\tau_1 \dots \tau_7$ (Table III) with corresponding relative contributions $A_1 \dots A_6$ or $A_1 \dots A_7$. This classification is just for convenience and does not automatically mean that, for instance, all τ_3 values in the table are identical (compare τ_3 of GFAP at 0.2 mM and 2.5 mM MgCl_2). At MgCl_2 concentrations higher than 2.5 mM, CONTIN (showing a broad distribution of decay times) and DISCRETE are not able to resolve the decay processes adequately (data not shown). However, up to 2.5 mM MgCl_2 well defined and mutually consistent decay times are produced by CONTIN and DISCRETE, CONTIN giving fully resolved distributions around the average decay times of DISCRETE. This is illustrated in Fig. 3 for GFAP at 2.5 mM MgCl_2 , where a good description requires decay times of approximately 40, 100, and 430 μs . Apparently, up to 2.5 mM MgCl_2 , a limited number of species are present in the solution.

For vimentin at 0 mM MgCl_2 , two major decay processes ($1.2 \pm 0.8 \mu\text{s}$ (τ_1) and $5.3 \pm 1.3 \mu\text{s}$ (τ_2)), and a small contribution (<4%) of a longer component ($24 \pm 8 \mu\text{s}$) (Table II) are found. In our previous studies on vimentin at pH 6.8 and 8.5 in the absence of MgCl_2 (6, 24), we found that decay times of 0.3–2.0 μs can be assigned to dimers of approximately 45 nm in length with a flexible and/or bent structure and that decay times of 4.0–7.0 μs can be assigned to staggered particles (probably tetramers and hexamers, possibly also octamers) with a length of 60–70 nm. Therefore, we conclude that, as at pH 6.8, vimentin at pH 7.5 without MgCl_2 is mainly present as single dimers and staggered particles. At 0.3 mM MgCl_2 , the decay times are almost identical to those in the absence of MgCl_2 , suggesting that the average length of the particles does not change.

Also for GFAP at 0 or 0.2 mM MgCl_2 , a decay time of $5.5 \pm 1.5 \mu\text{s}$ is found (Table III). As for vimentin, we assign this to staggered particles (probably tetramers and hexamers, possibly also octamers) with a length of 60–70 nm. However, addi-

tionally, a small component with a decay time of $17 \pm 4 \mu\text{s}$ is detected (Table III), showing that larger aggregates are already formed in the absence of MgCl_2 . The shortest decay time of GFAP (τ_1 in Table III) has been described and analyzed before (7) and is probably not due to dimers but arises from a bent and/or flexible higher oligomer. This can explain the lower value for S_1/S_2 in comparison with vimentin, since fewer dimers means a lower permanent dipole moment contribution to the orientation mechanism of the particles.

At higher MgCl_2 concentrations, the average TEB decay time (τ_{av}) becomes much larger (see Fig. 2), whereas addition of NaCl (not shown) had no effect on τ_{av} . For vimentin, formation of larger aggregates starts at 0.5 mM MgCl_2 . A “new” component with a decay time of $26 \pm 5 \mu\text{s}$ (τ_3) and a relative contribution of approximately 27% (see Table II) appears, but a significant fraction of dimers and staggered structures (τ_1 and τ_2) is still present. τ_1 and τ_2 disappear at higher concentrations of MgCl_2 , and a gradual shift to longer decay times due to larger particles (τ_3 , τ_4 , and τ_5) is observed. At 1.8 and 2.5 mM MgCl_2 , two major decay times, around 40 and 110 μs , are found. The 40- μs component is intermediate between τ_3 and τ_4 as obtained at lower MgCl_2 concentrations and might be an unresolved average of the two. Alternatively, it is due to a flexibility mode of higher oligomers.

For GFAP, a similar pattern with almost identical decay times as for vimentin is observed (Table III, Fig. 2), but assembly occurs at lower MgCl_2 concentrations. Larger structures are formed at 0.3 mM MgCl_2 , where τ_1 and τ_2 are no longer observed. Above 1.0 mM MgCl_2 , the shortest decay time (τ_3) reflects either the average of τ_3 and τ_4 measured at lower MgCl_2 concentrations or flexibility of higher order aggregates. At 2.0 and 2.5 mM MgCl_2 , a very long decay time of approximately 430 μs is observed (τ_7 in Table III), which is not detected in the case of vimentin. In Table IV, the weighted average values

TABLE I

Kerr constants for 1 M protein chain and S_1/S_2 values of vimentin and GFAP at different MgCl_2 concentration

The resistance of the solution was adjusted to 200 Ω (see “Experimental Procedures”).

protein	[MgCl_2]	Pulse length	S_1/S_2	K
	<i>mM</i>	μs		$\times 10^{-13} \text{ m}^2 \text{ V}^{-2}$
Vimentin	0	70	2.1 ± 0.1	1.2 ± 0.2
Vimentin	0.3	70	1.1 ± 0.1	0.9 ± 0.2
Vimentin	0.5	200	1.1 ± 0.1	4.0 ± 1.0
Vimentin	1.0	500	1.1 ± 0.1	13.2 ± 1.3^a
GFAP	0	140	1.5 ± 0.2	1.4 ± 0.3
GFAP	0.2	140	1.2 ± 0.1	1.4 ± 0.3
GFAP	0.3	500	1.1 ± 0.1	12.4 ± 0.8
GFAP	0.5	500	1.1 ± 0.1	17.0 ± 1.1

^a Corrected value (see “Experimental Procedures”).

TABLE II

TEB decay analysis after electric field pulses of vimentin at various concentrations of MgCl_2 by CONTIN and DISCRETE

Decay times (τ) and their relative contributions (A) assigned to distinct oligomeric species with a relative contribution >10% are denoted in boldface type; decay times with a relative contribution <10% are denoted in italics. Pulse length was 70 μs .

[MgCl_2]	A_1	τ_1	A_2	τ_2	A_3	τ_3	A_4	τ_4	A_5	τ_5	A_6	τ_6
<i>mM</i>	%	μs	%	μs	%	μs	%	μs	%	μs	%	μs
0 ^a	48 ± 5	1.2 ± 0.8	48 ± 5	5.3 ± 1.3	<4	<i>24 ± 8</i>						
0.3 ^a	52 ± 6	1.2 ± 0.8	44 ± 6	5.5 ± 1.5	<6	<i>30 ± 10</i>						
0.5 ^b	13 ± 4	1.4 ± 0.5	60 ± 8	5.5 ± 1.5	27 ± 12	26 ± 5						
1.0 ^b			<10	<i>4.0 ± 2.0</i>	75 ± 8	29 ± 8	25 ± 6	70 ± 17				
1.4 ^b					35 ± 7	33 ± 7	55 ± 5	60 ± 10			<10	<i>170 ± 50</i>
1.8 ^b					<i>60 ± 10^c</i>	<i>44 ± 5^c</i>			35 ± 7	120 ± 15	<5	<i>250 ± 50</i>
2.5 ^b					<i>45 ± 8^c</i>	<i>42 ± 6^c</i>			50 ± 8	110 ± 15	<5	<i>250 ± 50</i>

^a Sample interval was 0.1 μs .

^b Sample interval was 0.5 μs .

^c Decay times not assigned to distinct oligomeric species but to a bent/flexible structure (see “Results”).

TABLE III

TEB decay analysis of GFAP at various concentrations of MgCl_2 by CONTIN and DISCRETE

Decay times (τ) and their relative contributions (A) assigned to distinct oligomeric species with a relative contribution >10% are denoted in boldface type; decay times with a relative contribution <10% are denoted in italics. Pulse length was 140 μs .

[MgCl_2]	A_1	τ_1	A_2	τ_2	A_3	τ_3	A_4	τ_4	A_5	τ_5	A_6	τ_6	A_7	τ_7
<i>mM</i>	%	μs	%	μs	%	μs	%	μs	%	μs	%	μs	%	μs
0 ^a	<i>35 ± 5^b</i>	<i>1.0 ± 0.4^b</i>	45 ± 5	6.0 ± 1.0	20 ± 10	17 ± 4								
0.2 ^a	<i>30 ± 7^b</i>	<i>1.0 ± 0.5^b</i>	40 ± 5	5.5 ± 0.8	20 ± 8	17 ± 4	<5	<i>55 ± 15</i>						
0.3 ^a					70 ± 6	30 ± 3	30 ± 6	66 ± 5			<2	<i>170 ± 50</i>		
0.5 ^c					52 ± 5	29 ± 5	45 ± 5	75 ± 8			<3	<i>240 ± 50</i>		
1.0 ^c					<i>67 ± 10^b</i>	<i>44 ± 5^b</i>			30 ± 7	120 ± 15			<3	<i>400 ± 50</i>
2.0 ^d					<i>40 ± 5^b</i>	<i>40 ± 6^b</i>			43 ± 4	104 ± 15			17 ± 9	440 ± 30
2.5 ^d					<i>25 ± 4^b</i>	<i>37 ± 3^b</i>			61 ± 4	96 ± 8			14 ± 8	430 ± 20

^a Sample interval was 0.2 μs .

^b Decay times not assigned to distinct oligomeric species but to a bent/flexible structure (see “Results”).

^c Sample interval was 0.5 μs .

^d Sample interval was 1.0 μs .

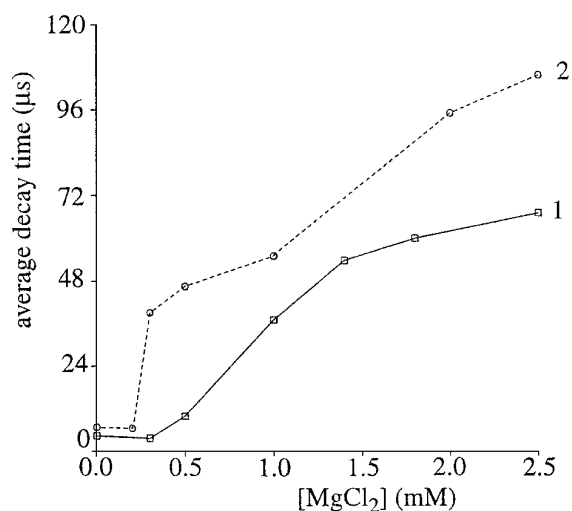


FIG. 2. Average (monoexponential) decay time of vimentin (1) and GFAP (2) as a function of MgCl_2 concentration. The pulse length was 70 μs (1) or 140 μs (2).

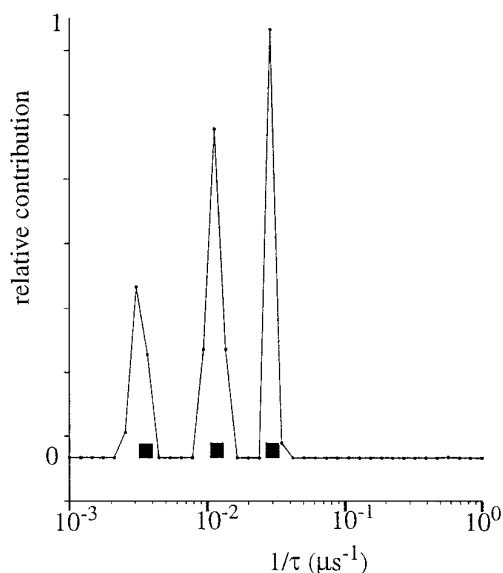


FIG. 3. CONTIN (continuous distribution; line) and DISCRETE (squares) analyses of GFAP in the presence of 2.5 mM MgCl_2 ; $E = 0.8$ kV/cm; pulse length, 140 μs .

of the various relaxation times with their assignments are given. We do not use decay times with a relative contribution less than 10% in the calculation, since their precise value is difficult to estimate.

DISCUSSION

The Absence of MgCl_2

We have shown before (6) that vimentin at pH 6.8 in the absence of MgCl_2 exists as single dimers approximately 45 nm in length and staggered structures of ~ 65 nm. At least part of the latter were shown to possess a relatively large overall dipole moment, which appeared to be compatible with the coexistence of ~ 65 -nm-long antiparallel staggered tetramers (or octamers) with relatively small permanent dipole moment and hexamers with a similar length and a relatively large permanent dipole moment. The decay times and S_1/S_2 values of vimentin at pH 7.5 in the absence of MgCl_2 (Tables I and II) are comparable with those observed at pH 6.8 (6). Therefore, we conclude that vimentin in the absence of MgCl_2 at pH 7.5 also forms single dimers (τ_1) as well as staggered tetramers (and/or

TABLE IV

Average-relaxation times (τ_{av}) (μs) and their assignment in vimentin and GFAP

Weighted averages of the relaxation times of Tables II and III per assigned class are given according to the equation,

$$\tau_{\text{av}} = \left(\sum_{i=1}^N \tau_i \cdot \sigma_i^{-2} \right) \left(\sum_{i=1}^N \sigma_i^{-2} \right)^{-1}$$

with i representing number of measurements, N representing total amount of measurements and σ_i representing error in τ_i .

	τ_{av} vimentin	τ_{av} GFAP	Assignment ^a
	μs	μs	
τ_{1A}	1.3 ± 0.4		Dimer rotation and flexibility
τ_{1B}		1.0 ± 0.3	Flexibility of higher oligomer
τ_2	5.4 ± 1.0	5.7 ± 0.8	Rotation staggered ~ 65 -nm building block
τ_{3A}		17 ± 4	Particle with length ~ 100 nm and relatively small diameter (< 5 nm)
τ_{3B}	28 ± 4	30 ± 3	Smallest full-width particle (~ 100 -nm length)
τ_{3C}	43 ± 4	39 ± 2	Flexibility of higher aggregate or average
τ_4	63 ± 9	69 ± 4	Second full-width particle (~ 135 -nm length)
τ_5	115 ± 11	102 ± 6	Third full-width particle (~ 170 -nm length)
τ_6			
τ_7		433 ± 17	Rotation or flexibility of very large filament structures

^a see Results and Discussion for assignments.

^b the relative contribution of this decay time was $< 10\%$ and is not included in this table (see "Results").

octamers) and hexamers with a length around 65 nm (τ_2). A comparable result has been found by Herrmann *et al.* (25). The value of τ_1 is the average of two decay times due to end-over-end rotation of the dimer and its bent and/or flexible structure (for a detailed analysis, see Ref. 24). This component is poorly defined in this experiment, since the sample interval of 0.1 μs is too large to detect both decay processes separately (24). Only a minor fraction of the decay curve ($< 4\%$) is due to larger aggregates (Table II). Very similar values for τ_1 and τ_2 are found for GFAP (Table III). However, in this case τ_1 is more likely to represent a bending or flexibility mode of a longer aggregate (7).

Very Low Concentrations of MgCl_2

In this study, we demonstrate that MgCl_2 -induced assembly of vimentin and GFAP occurs in a number of more or less discrete structural intermediates. A physiological pH value (7.5) was chosen for vimentin polymerization, while for GFAP a pH value of 6.8 (based on the work of Inagaki *et al.* (38)) was taken. At 0.3 mM MgCl_2 for vimentin and 0.2 mM MgCl_2 for GFAP, decay components are similar to those found in the absence of MgCl_2 . However, the permanent dipole moment as observed in the absence of MgCl_2 almost disappears ($S_1/S_2 = 1.1 \pm 0.1$), while the Kerr constant slightly decreases for vimentin (Table I). These results can be explained by the disappearance of ~ 65 -nm-long hexamers (possessing a permanent dipole moment) at the expense of antiparallel ~ 65 -nm-long tetramers and/or octamers (permanent dipole moments of constituting particles cancel). In addition, the disappearance of the dipole moment may partly be due to the binding of Mg^{2+} to the protein, leading to a compensation of its negative charges (24).

Higher Concentrations of MgCl_2

Increasing the MgCl_2 concentration further leads to a sharp increase of the decay times and Kerr constants, which demonstrates that larger aggregates are formed. The dominating species at 1.0 mM MgCl_2 in the case of vimentin has a decay time of 28 μs (average value of τ_{3B} in Table IV) besides a minor

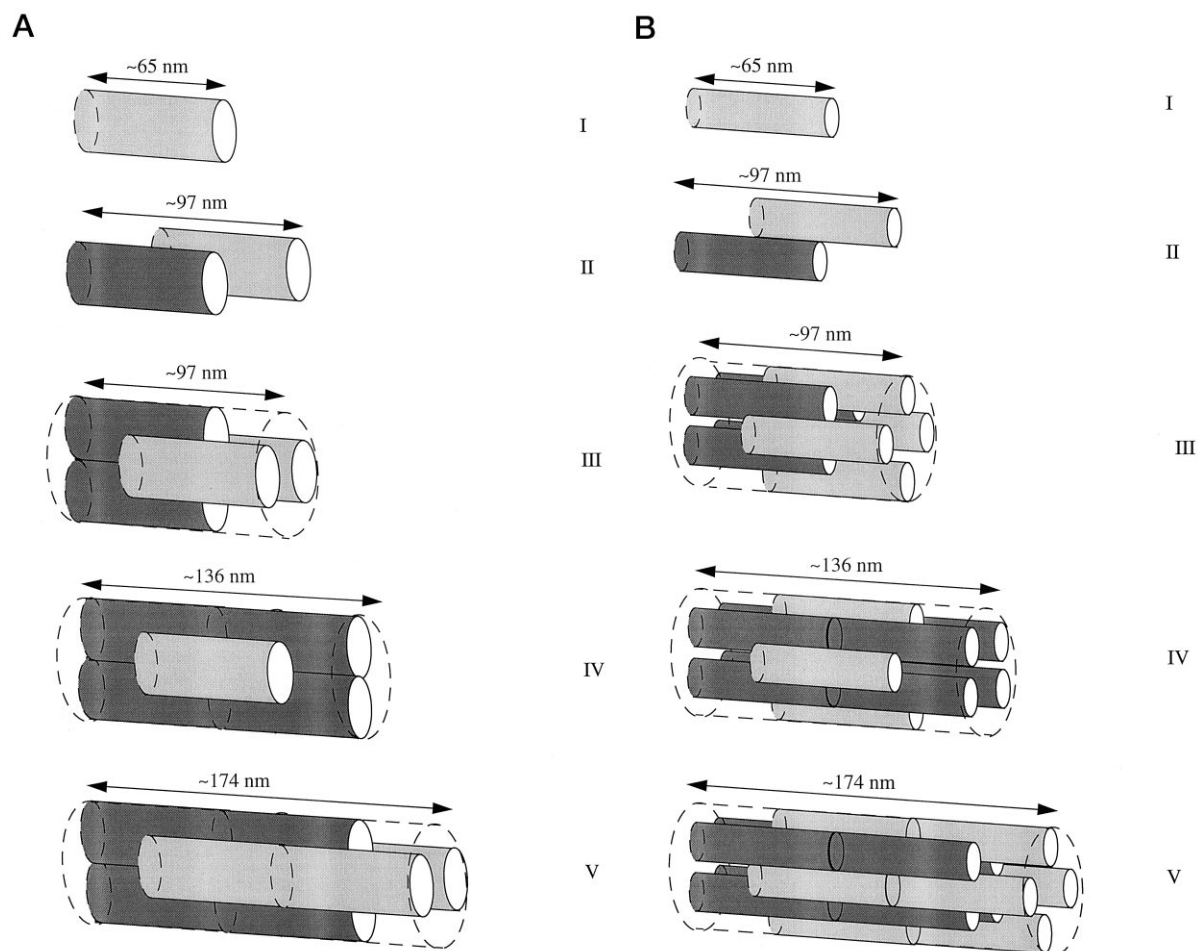


FIG. 4. *A*, a model for vimentin and GFAP IF formation, assuming that an octamer is the basic building block. *I*, octamer; *II*, ~100-nm aggregate; *III*, smallest full-width particle; *IV* and *V*, elongation of the particle shown in *III* by the subsequent addition of two octamers. This model accounts for the observed TEB decay times and Kerr constants at different MgCl_2 concentrations. *B*, a model for IF formation from tetrameric building blocks. *I*, tetramer; *II*, ~100-nm aggregate; *III*, smallest full-width particle; *IV* and *V*, elongation of the particle shown in *III* by the subsequent addition of four tetramers. This model also accounts for the observed TEB decay times and Kerr constants at different MgCl_2 concentrations.

component of $63 \mu\text{s}$ (average value of τ_4 in Table IV). The relative contributions of the components change upon going from 0.5 to 1.4 mM where the longer decay times start to contribute more, but the well defined and more or less constant decay times show that IF assembly occurs via a specific pathway rather than random lateral and/or longitudinal growing of aggregates. Upon going from 0 to 1.0 MgCl_2 , K increases from $1.2 \times 10^{-13} \text{ m}^2\text{V}^{-2}$ to $13.2 \times 10^{-13} \text{ m}^2\text{V}^{-2}$ for 1 M protein chain. As is demonstrated in the Appendix, this increase of the Kerr constant shows that the 28- μs vimentin particles contain at least 31 ± 8 monomeric units.

The 28- μs Component

Full-width IF particles under equilibrium conditions contain about 32 monomeric units in cross-section and have a diameter of about 10 nm (1, 13, 14, 23, 25, 28). A rigid particle of 10-nm diameter and 65-nm length would give rise to a decay time of approximately $10 \mu\text{s}$ (30–32). Neither for vimentin nor for GFAP is such a decay time observed. Polymerization of vimentin seems to proceed directly from a 5.5- μs complex to a 28- μs complex, and these complexes coexist in varying ratios at different salt concentrations.

Also, the possibility of a head-to-tail arrangement of the 65-nm building blocks in the 28- μs component can be excluded. In that case, the complex would be 130 nm long, and since it contains at least 31 ± 8 monomeric units, it must have at least 16 ± 4 monomers in cross-section. Since the diameter of tet-

ramers is ~ 2.5 nm (9), the diameter of such a 130-nm complex would be at least 5 nm. This would lead to a decay time of approximately $40 \mu\text{s}$ (30–32), which is clearly too high. Therefore, we conclude that the 28- μs oligomers are not 65 nm, full-width particles; nor are they formed by head-to-tail arrangement of the 65-nm building blocks into 130-nm particles. Clearly, the length is in between. Hence, significant spatial overlap must exist between the 65-nm building blocks in the 28- μs particles. Thus, at least a significant part of the complex contains the 31 ± 8 monomeric units in cross-section, and the 28- μs particles are at least for a significant part full-width aggregates with a length that exceeds the 65 nm of the building blocks. Two possible global models for this complex are given in Fig. 4, *A* and *B* (part *III*), where an octamer and a tetramer have been taken as a building block, respectively. Using a full-width of 10 ± 2 nm (13, 14), one can calculate a length of 97 ± 6 nm for this particle (30–32). A similar calculation for the 30- μs particle of GFAP leads to a length of 100 ± 4 nm.

The 17- μs Component

Only for GFAP at low salt concentrations did we also observe a 17- μs component. This decay time cannot be due to lateral aggregation of 65-nm particles, since this would lead to a decay time of $10 \mu\text{s}$ (see above). However, it can be due to two staggered 65-nm building units (tetramers or octamers) with a total length of ~ 100 nm and a diameter of ~ 5 nm. This particle is depicted in Fig. 4, *A* and *B* (part *II*).

Larger Particles

Assuming a diameter of 10 nm, the next steps in IF assembly lead to lengths of $136 \pm 8/142 \pm 4$ nm (τ_4) and $174 \pm 6/166 \pm 4$ nm (τ_5) for vimentin and GFAP, respectively. Apparently, longitudinal growth of vimentin IFs from 65 to 174 occurs in discrete steps of approximately 35 nm. Further elongation of vimentin is impossible to follow quantitatively, due to large uncertainties in the analysis (see "Results"). For GFAP, the next discrete relaxation time is 433 ± 17 μ s. This time corresponds to a cylinder length of 292 ± 3 nm, which is slightly less than twice the length of the 166 ± 4 structure represented by τ_5 . We are hesitant to put too much emphasis on this decay time, since the plateau value of the birefringence during the pulse was not completely reached.

A Structural Model for IF Assembly

The General Model—The results lead us to the model for group III IF assembly given in Fig. 4, A and B. Flexible dimers form antiparallel more or less rigid tetramers, which entwine to octamers that have been assumed to be the ~ 65 -nm building blocks in Fig. 4A (τ_2). The process of thickening to full-width particles requires partial overlap of these building blocks to 100-nm-long aggregates (possibly τ_{3A} in Table IV), which then rapidly form full-width particles (τ_{3B} in Table IV). In vimentin, the intermediate form reflected by τ_{3A} could not be detected, but we found some evidence for its existence before (6). The minimum number of 31 ± 8 monomers in the ~ 100 -nm particle implies the presence of at least 4 ± 1 octamers in this smallest stable full-width aggregate. The next two elongation steps (τ_4 and τ_5) then presumably each add another two octamers in a staggered way to the growing filament. In this model we implicitly assume that GFAP and vimentin aggregate in a similar way (most relaxation times are almost identical, as is the increase in K). However, the tendency for aggregation is stronger for GFAP at pH 6.8 than for vimentin at pH 7.5 (GFAP in 0.3 mM $MgCl_2$ is comparable with vimentin in 1.0 mM $MgCl_2$). In addition, GFAP shows an intermediate step between the octameric form and the full-width 100-nm particles.

Assuming tetramers to be the ~ 65 -nm structural units in the assembly of IF proteins, and following the argument given above, the model of Fig. 4B is obtained. In this case, the ~ 100 -nm aggregate contains 8 ± 2 tetramers, and the next steps add four tetramers each to the protein aggregate. At this stage, we cannot discriminate between the two models. Of course, our models are extremely simplified, and one should probably consider these discrete intermediates as the average of a narrow distribution of complexes with a similar length and width.

Calculation of Relative Amounts of Different Types of Aggregates—From point 3 of the "Theoretical Background" it can be seen that the relative amplitudes of the decay times in Table II and III have to be divided by the Kerr constants of the various species to obtain the relative concentrations of these species. For T-vimentin, it was estimated (24) that the ratio of the K values for dimers and tetramers is 0.57, and one might expect this ratio to be rather similar for vimentin. However, we cannot determine the relative concentrations of tetramers, hexamers, and III octamers, since they all give rise to a similar decay time. Hence, it is not possible to estimate the relative occurrence of dimers and tetramers accurately. Therefore, we do not discriminate and use a single average Kerr constant for dimers, tetramers, hexamers, and octamers. Although this is a very crude approximation, it hardly influences the estimates of the ratio of the concentrations of oligomers (dimers up to octamers) and larger aggregates (see below). A drastic change in the height of the signals and thus of the Kerr constant occurs when

type III complexes (Roman numbers correspond to the numbering in Fig. 4, A and B) are formed, and we estimate the value of K for type III complexes to be 10 times as high (see "Results" and the Appendix) as that of the small oligomers (the mixture of dimers, tetramers, hexamers, and octamers). As dipolar properties from the larger aggregates do not change, their Kerr constants will be more or less linear with the mass, and the K values of type II, IV, and V complexes can be assumed to be 0.5, 1.5, and 2.0 times the K of type III particles.

Vimentin—Using our model and applying the consideration of the previous paragraph we are now able to interpret Tables II and III in more detail. For vimentin (Table II) in the absence of Mg^{2+} , both dimers and hexamers are present and probably coexist with tetramers/octamers. Hexamers have disappeared in 0.3 mM Mg^{2+} . At 0.5 mM Mg^{2+} , the relative occurrence of dimers has also diminished significantly, and some type III structures are observed. Taking into account the relative K values, their relative amount is roughly 20 times lower than that of tetramers/octamers. At 1.0 mM Mg^{2+} , type III structures dominate the birefringence, but tetramers/octamers and type IV aggregates are also present. Taking into account the relative K values, the amounts of tetramers/octamers and type III species are comparable, whereas the ratio of type III to type IV can be estimated to be 4:1. At 1.4 mM Mg^{2+} , no small oligomers can be observed anymore, although some of them might still be present. The decay signals are dominated by type III and type IV complexes, and their relative concentrations are estimated to be equal. At 1.8 and 2.5 mM Mg^{2+} type V structures are also present. Recalling from the results that the decay time of ~ 43 μ s is possibly due to an average of the decay times of type III (decay time 28 μ s) and type IV (decay time 63 μ s) particles, the relative amount of the type V structures at 1.8 and 2.5 mM Mg^{2+} can be estimated to be 20–30 and 35–45%, respectively.

GFAP—For GFAP (Table III), the situation is slightly different. It was mentioned before that in the absence of Mg^{2+} , hexamers and tetramers/octamers (but most likely no dimers) coexist with type II structures that were not observed for vimentin. We estimate the relative amount of the type II structures to be $\sim 10\%$ at most. At 0.2 mM Mg^{2+} , hexamers have disappeared to a large extent, but the relative amount of type II structures remains unchanged. At 0.3 mM Mg^{2+} the signal is suddenly dominated by type III and type IV structures in relative amounts of 80 and 20%, respectively. As was discussed above for vimentin, we cannot rule out that still some smaller oligomers are present. At 0.5 mM Mg^{2+} , the relative amount of type III and IV structures changed to 65 and 35%, respectively. At 1.0 mM, type V structures start to appear, whereas the 44- μ s component is probably due to a mixture of type III and IV structures. The relative amount of type V complexes is estimated to be 15–25%. At 2.0 mM Mg^{2+} , longer complexes also start to appear (τ_7), but type III, IV, and V structures dominate. At 2.5 mM, the amount of type III and type IV structures is even smaller. Since we cannot really assign τ_7 , we cannot estimate the relative amounts at the highest salt concentrations.

Comparison with Existing Models—The presented model, in which a rapid increase of the diameter of the filaments is followed by slower elongation, is in agreement with the interpretation of turbidity experiments on vimentin (40) and GFAP (41). In these stopped-flow studies, a fast initial increase of turbidity followed by a much slower rise to a plateau value was observed. The fast increase was tentatively associated with an increase in thickness, and the slow rise was associated with lengthening of the aggregates. Our present work is roughly in agreement with this interpretation, but we are able to show that an increase in width is accompanied by a limited increase in length (to ~ 100 nm). In the case of GFAP, this length seems

to be reached before the full width has been obtained, and in view of the similarity of the entire aggregation process for vimentin and GFAP, this might also be the case for vimentin. Elongation of full-width particles occurs via discrete steps of ~35 nm.

Our results are not compatible with results of Herrmann *et al.* (25), who observed first a thickening of human vimentin to full-width particles with a diameter of approximately 10 nm and a length of 65 nm under comparable conditions. As was mentioned above, this would lead to a decay time of ~10 μ s, which is clearly absent in our measurements. Under nonequilibrium conditions, Herrmann *et al.* (25) found (by rapid dilution in filament-forming buffer, addition of glutaraldehyde, and negative staining) average diameters of approximately 16 nm. Using this diameter in our calculations, the lengths of the intermediate aggregates would be close to 85, 125, and 155 nm. However, in their experiments they also observe complexes with a diameter of 16 nm and a length of 65 nm, which would lead to a decay time of ~13 μ s in our experiments. Such a time is not in disagreement with a decay time of 17 ± 4 μ s as observed for GFAP, but given the small contribution of this component it is clear that aggregates with such a large diameter are not being formed in significant amounts and are certainly not present for vimentin. Possibly, the difference between the results of Herrmann *et al.* (25) and ours is caused by their use of nonequilibrium conditions.

APPENDIX

Estimation of Number of Monomers in the 28- μ s Vimentin Particle

The ratio of the Kerr constants for vimentin tetramers (K_{tet}) and aggregates (K_{agg}) is given by the equation,

$$K_{tet}/K_{agg} = (P_{tet} + Q_{tet})/(P_{agg} + Q_{agg}) \quad (\text{Eq. 3})$$

(see also Ref. 24). The induced dipole moment contribution can be split into a term due to internal charge distribution of the complex (Q_i) and a term representing the contribution of counterions (Q_e). The former is proportional to the number of monomeric units of the complex (*i.e.* to its mass), whereas the latter depends more or less on the surface area. In the absence of $MgCl_2$, particles having both a permanent and induced dipole moment (dimers and hexamers) and particles without a permanent dipole moment (tetramers and/or octamers) are present (6, 24). Raising the $MgCl_2$ concentration from 0 to 1.0 mM increases K with a factor of 11.5 ± 3.0 (Table I), whereas the dominating relaxation time becomes 28 μ s (Table IV). To get an estimate of the number (N) of monomeric units in the particles corresponding to this decay time, we will calculate some simple cases.

First, we assume that in the absence of $MgCl_2$ only antiparallel tetramers without dipole moment (thus $P_{tet} = 0$) are present, whereas at 1 mM $MgCl_2$ there is exclusively the 28- μ s component (also without a permanent dipole moment ($P_{agg} = 0$)). Then

$$K_{tet}/K_{agg} = (Q_i(tet) + Q_e(tet))/(Q_i(agg) + Q_e(agg)) = 1/(11.5 \pm 3.0) \quad (\text{Eq. 4})$$

and thus

$$Q_i(agg) + Q_e(agg) = (11.5 \pm 3.0) \times (Q_i(tet) + Q_e(tet)) \quad (\text{Eq. 5})$$

Substituting $Q_i(agg) = (N/4)Q_i(tet)$ yields

$$(N/4) \times Q_i(tet) + Q_e(agg) = (11.5 \pm 3.0) \times (Q_i(tet) + Q_e(tet)) \quad (\text{Eq. 6})$$

If Q_e were proportional to the mass, $Q_e(agg)$ would equal $(N/4)Q_e(tet)$. Substituting this in Equation 6 yields $(N/4) = 11.5 \pm 3.0$; thus, $N = 46 \pm 12$. However, since Q_e is more or less proportional to the surface area, $Q_e(agg) \leq (N/4)Q_e(tet)$; thus,

$N \geq 46 \pm 12$. If at 0 mM $MgCl_2$, only octamers are present, a similar calculation yields more than 92 ± 24 monomeric units in the aggregate.

The calculation is slightly different if it is assumed that exclusively dimers are present in the absence of $MgCl_2$, since these particles have both an induced and a permanent dipole moment. Since K is proportional to $P + Q$, then, assuming the ratio between the Kerr constants of vimentin dimers and tetramers to be equal to that of T-vimentin (0.57; see Ref. 24), the following is true,

$$Q_i(agg) + Q_e(agg) = (11.5 \pm 3.0) \times (Q_i(dim) + Q_e(dim) + P_{dim}) \quad (\text{Eq. 7})$$

or

$$(N/4) \times Q_i(tet) + Q_e(agg) = (11.5 \pm 3.0) \times (Q_i(tet) + Q_e(tet)) \quad (\text{Eq. 8})$$

This implies that in this case $N \geq 26.2 \pm 6.8$.

To estimate a minimum number of monomers in the 28- μ s particles, we first assume that in the absence of $MgCl_2$ only dimers and antiparallel tetramers (without a permanent dipole moment) are present. The amplitude of the Kerr signal depends on both the concentration of the particles and their birefringent properties. To calculate the concentration of dimers and tetramers, we equalize the contribution of their birefringent properties by multiplying the amplitude of the tetramers by the ratio of the Kerr constants of dimers and tetramers, again assuming that this value for vimentin is equal to that of T-vimentin (0.57; see Ref. 24). Hence, the corrected amplitudes for tetramers and dimers are $0.57 \times 48 = 27$ and 48 (see Table II) of the complex, respectively, and their relative occurrence is $27/(27 + 48) = 0.36$ and $48/(27 + 48) = 0.64$, respectively. Using these figures and the results for N derived above, it can be concluded that a minimum of 33 ± 9 monomers are present in the 28- μ s particles. However, in this calculation we have neglected the contribution of the 63- μ s particle (τ_4). This leads to an overestimation of the lower limit of N by approximately 7%. Thus, the 28- μ s particles consist of at least 31 ± 8 monomers. When, in addition to antiparallel tetramers, hexamers and/or octamers are present, this number increases to 37 ± 10 at most. Using the extreme values for K_{dim}/K_{tet} (24) or the amplitudes of dimers and tetramers (Table II) does not change the numbers significantly. Also, using the results obtained in the presence of 0.3 mM $MgCl_2$ instead of those obtained in the absence of $MgCl_2$ gives similar results.

REFERENCES

- Fuchs, E. & Weber, K. (1994) *Annu. Rev. Biochem.* **63**, 345–382
- Heins, S. & Aebi, U. (1994) *Curr. Opin. Cell. Biol.* **6**, 25–33
- Quinlan, R. A. & Franke, W. W. (1982) *Proc. Natl. Acad. Sci. U. S. A.* **97**, 3452–3456
- Kaufmann, E., Weber, K. & Geisler, N. (1985) *J. Mol. Biol.* **185**, 733–742
- Quinlan, R. A., Hatzfeld, M., Franke, W. W., Lustig, A., Schulthess, T. & Engel, J. (1986) *J. Mol. Biol.* **192**, 337–349
- Kooijman, M., Bloemendal, M., van Amerongen, H., Traub, P. & van Grondelle, R. (1994) *J. Mol. Biol.* **236**, 1241–1249
- Kooijman, M., van Amerongen, H., Traub, P., van Grondelle, R. & Bloemendal, M. (1995) *FEBS Lett.* **358**, 185–188
- Ip, W., Hartzler, M. K., Susana Pang, Y.-Y. & Robson, R. M. (1985) *J. Mol. Biol.* **183**, 365–375
- Potschka, M., Nave, R., Weber, K. & Geisler, N. (1990) *Eur. J. Biochem.* **190**, 503–508
- Steinert, P. M. (1991) *J. Struct. Biol.* **107**, 157–174
- Steinert, P. M. (1991) *J. Struct. Biol.* **107**, 175–188
- Geisler, N., Schünemann, J. & Weber, K. (1992) *Eur. J. Biochem.* **206**, 841–852
- Aebi, U., Fowler, W. E., Rew, P. & Sun, T.-T. (1983) *J. Cell. Biol.* **97**, 1131–1143
- Aebi, U., Häner, M., Troncoso, J., Eichner, R. & Engel, A. (1988) *Protoplasma* **145**, 73–81
- Steinert, P. M. & Roop, D. R. (1988) *Annu. Rev. Biochem.* **57**, 593–625
- Eichner, R., Rew, P., Engel, A. & Aebi, U. (1985) *Annu. N. Y. Acad. Sci.* **455**, 381–402
- Geisler, N. (1993) *FEBS Lett.* **323**, 63–67
- Steinert, P. M. & Parry, D. A. D. (1993) *J. Biol. Chem.* **268**, 2878–2887
- Steinert, P. M., Marekow, L. N., Fraser, R. D. B. & Parry, D. A. D. (1993) *J. Mol. Biol.* **230**, 436–452

20. Steinert, P. M., Marekow, L. N. & Parry, D. A. D. (1993) *Biochemistry* **32**, 10046–10056
21. Steinert, P. M., Marekow, L. N. & Parry, D. A. D. (1993) *J. Biol. Chem.* **268**, 24916–24925
22. Heins, S., Wong, P. C., Müller, S. A., Goldie, K., Cleveland, D. W. & Aebi, U. (1993) *J. Cell. Biol.* **123**, 1517–1533
23. Parry, D. A. D. (1995) *Proteins Struct. Funct. Genet.* **22**, 267–272
24. Kooijman, M., Bloemendal, M., Traub, P., van Grondelle, R. & van Amerongen, H. (1995) *J. Biol. Chem.* **270**, 2931–2937
25. Herrmann, H., Häner, M., Brettel, M., Müller, S. A., Goldie, K. N., Fedtke, B., Lustig, A., Franke, W. W. & Aebi, U. (1996) *J. Mol. Biol.* **264**, 933–953
26. Stewart, M., Quinlan, R. A. & Moyer, R. D. (1989) *J. Cell Biol.* **109**, 225–234
27. Vorgias, C. E. & Traub, P. (1983) *Biochem. Biophys. Res. Commun.* **115**, 68–75
28. Weast, R. C. (ed) (1971) *Handbook of Chemistry and Physics*, 52nd Ed. pp. C528–C529, Chemical Rubber Co., Cleveland, OH
29. Fredericq, E. & Houssier, C. (1973) in *Electric Dichroism and Electric Birefringence* (Harrington, W., and Peacocke, A. R., eds) Clarendon Press, Oxford
30. Broersma, S. (1960) *J. Chem. Phys.* **32**, 1626–1631
31. Broersma, S. (1981) *J. Chem. Phys.* **74**, 6989–6990
32. Mandelkern, M., Elias, J. G., Eden, D. & Crothers, D. M. (1981) *J. Mol. Biol.* **152**, 153–161
33. Van Haeringen, B., Jiskoot, W., van Grondelle, R. & Bloemendal, M. (1992) *J. Biomol. Struct. & Dyn.* **9**, 991–1011
34. Provencher, S. W. (1976) *Biophys. J.* **16**, 27–41
35. Provencher, S. W. (1976) *J. Chem. Phys.* **64**, 2772–2777
36. Provencher, S. W. (1982) *Comp. Phys. Commun.* **27**, 213–227
37. Provencher, S. W. (1982) *Comp. Phys. Commun.* **27**, 229–242
38. Inagaki, M., Gonda, Y., Nishizawa, K., Kitamura, S., Sato, C., Ando, S., Tanabe, K., Kikuchi, K., Tsuiki, S. & Nishi, Y. (1990) *J. Biol. Chem.* **265**, 4722–4729
39. Parry, D. A. D. (1996) *Int. J. Biol. Macromol.* **19**, 45–50
40. Zakroff, R. V. & Goldman, R. D. (1979) *Proc. Natl. Acad. Sci. U. S. A.* **76**, 6226–6230
41. Yang, Z. W., Kong, C. F. & Babitch, J. A. (1988) *Biochemistry* **27**, 7045–7050